

## Highlights

### **Quantifying Particle and Wave Effects in Phonon Transport of Pillared Graphene Nanoribbons**

Shixian Liu, Zhicheng Zong, Fei Yin, V.I. Khvesyuk, Nuo Yang

- Quantified the contributions of particle and wave effects to the reduction in thermal conductivity of PGNRs.
- Identified a saturation behavior of wave effects as the PGNR width decreases.
- Introduced and evaluated the phonon resonance hybridization depth in PGNRs.

# Quantifying Particle and Wave Effects in Phonon Transport of Pillared Graphene Nanoribbons

Shixian Liu<sup>a,1</sup>, Zhicheng Zong<sup>b,c,1</sup>, Fei Yin<sup>a</sup>, V.I. Khvesyuk<sup>a,\*</sup>, Nuo Yang<sup>b,\*\*</sup>

<sup>a</sup>*Department of Thermophysics, Bauman Moscow State Technical University, Moscow, 105005, Russia*

<sup>b</sup>*Department of Physics, National University of Defense Technology, Changsha, 410073, China*

<sup>c</sup>*School of Energy and Power Engineering, Huazhong University of Science and Technology, Wuhan, 430074, China*

---

## Abstract

This study investigates the dual nature of phonons—encompassing both particle-like and wave-like behaviors—and their roles in thermal transport within pillared graphene nanoribbons (PGNRs). Monte Carlo simulations are employed to evaluate how the presence of pillars affects the thermal conductivity of graphene nanoribbons (GNRs), revealing that pillars significantly reduce thermal conductivity by enhancing phonon-boundary scattering, thereby emphasizing particle effects. A comparison with molecular dynamics simulations enables quantitative assessment of the respective contributions of particle and wave phenomena to the observed reduction in thermal conductivity. Notably, as the width of PGNRs decreases, the influence of wave effects initially increases and then diminishes, suggesting a saturation behavior. Furthermore, this study introduces and evaluates the concept of phonon resonance hybridization depth in PGNRs.

*Keywords:* Phonon particle effect, Phonon wave effect, Pillared graphene nanoribbons, Thermal conductivity, Monte Carlo, Molecular dynamics

---

\*Corresponding author

\*\*Principal corresponding author

Email addresses: 2636623@gmail.com (V.I. Khvesyuk), nuo@nudt.edu.cn (Nuo Yang)

<sup>1</sup>The two authors contributed equally to this work.

## 1. Introduction

Phonons, as energy carriers, exhibit both wave-like and particle-like properties. This duality plays a key role in determining a material’s thermal characteristics. While extensive research has focused on the particle and wave behavior of electrons and photons [1–4], the complex interplay between these properties in phonons remains a significant challenge [5, 6]. A deeper understanding of phonon transport is essential for advancing applications in thermal management [7, 8], including nanofluid-based solar collectors and heat transfer devices [9–11], thermal rectification [12, 13], and thermoelectric energy conversion [14–16].

Traditionally, controlling phonon transport has predominantly focused on their particle-like behavior. Techniques such as introducing rough edges [17–19], interfaces [20], pores [21], defects [22], and doping [23] have been employed to scatter phonons and thereby reduce thermal conductivity. In contrast, approaches leveraging the wave-like nature of phonons emphasize the role of phase information, interference, and resonance effects during coherent transport [24–28]. Coherent phonon transport in periodic structures can lead to localized resonances and the formation of standing waves, effectively disrupting phonon propagation at specific frequencies [29–35]. Notably, these control strategies are not limited to ideal crystalline materials but can also be applied to amorphous systems, where tuning phonon transport remains a key challenge [36, 37].

Graphene nanoribbons (GNRs) are particularly promising for applications such as transistors [38, 39], solar cells [40], and other electronic devices [41] due to their ability to open graphene’s bandgap. The thermal and electrical properties of GNRs can be fine-tuned by adjusting ribbon width and edge configurations [42–47]. Studying the thermal properties of GNRs is essential for enhancing device performance and gaining deeper insights into the physics of low-dimensional systems. Pillared graphene nanoribbons (PGNRs) exploit the wave-like nature of phonons to disrupt transport via local resonant hybridization, thereby reducing thermal conductivity [48, 49]. These studies have mainly focused on the wave behavior of phonons in PGNRs. At the same time, there is also a contribution to the reduction in thermal conductivity from phonon scattering at boundaries.

At the nanoscale, particle and wave effects must be treated separately to fully understand the thermal transport mechanism [50, 51]. Although previous studies have explored the dual behavior of phonons in systems such as

pillared nanowires [31] and nanoporous graphene [27], no work has quantitatively analyzed the particle and wave effects in PGNRs. Compared to silicon [31], phonons in graphene have much longer intrinsic mean free paths and are more sensitive to boundary modifications. While previous studies have focused on wave-like transport mechanisms—such as coherence and localization—in nanoporous graphene [27], they have not considered the unique structural and phononic characteristics of PGNRs. In PGNRs, periodic boundaries not only induce phonon resonance hybridization, altering dispersion relations, but also enhance boundary scattering, which reduces phonon mean free paths. These effects make PGNRs an ideal system for quantitatively examining the interplay between particle- and wave-like phonon transport.

The phonon Boltzmann transport equation (PBTE) has long served as a fundamental theoretical framework for calculating the thermal conductivity of semiconductors [52, 53]. With the development of density functional theory (DFT) [54, 55], which enables accurate approximate solutions to the many-body Schrödinger equation [56] via the Kohn–Sham formalism, it has become possible to solve the PBTE from first principles with high precision [57–60]. For micro- and nanoscale systems, numerical solutions of the PBTE [61, 62] or Monte Carlo (MC) methods [47] are often employed. It is important to note that the PBTE is inherently a particle-based formalism grounded in phonon scattering processes. In parallel, the advancement of atomistic simulation techniques has led to the widespread adoption of molecular dynamics (MD) [30, 63, 64], which directly models atomic vibrations and naturally captures both the particle-like and wave-like characteristics of phonons. This makes MD a powerful complementary approach for evaluating thermal conductivity, particularly in systems where wave effects are significant.

Theoretical studies [29–36] show that resonance caused by pillars can significantly reduce thermal conductivity, provided that the pillars are defect-free and in perfect contact with the body. Resonant frequencies align with the body’s phonon modes, leading to flat dispersion relations and lower group velocities. However, experimental measurements [65] indicate that such resonance effects are often negligible in practice due to structural imperfections. These imperfections lead to a reduced number of matched resonant frequencies and the formation of hybrid modes, ultimately diminishing the expected suppression of thermal transport. Furthermore, theoretical findings suggest that introducing defects or isotopic doping in the pillars weakens the re-

onance effect, leading to higher thermal conductivity than that of perfect structures [30, 66]. These findings highlight the critical role of structural perfection in realizing phonon resonance effects for effective thermal transport control.

This paper examines how pillars affect the thermal conductivity of GNRs by influencing both the wave and particle characteristics of phonons. Firstly, MC simulations are employed to capture the particle-like behavior of phonons, including phonon-phonon scattering and boundary scattering. Secondly, MD simulations are used to model the wave-like behavior of phonons, focusing on the interference and localization effects introduced by the pillars. Lastly, a comparison of the results from both methods is conducted to quantify the contributions of particle and wave effects to the reduction in thermal conductivity. The study further examines how the width of PGNRs and the pillar height influence phonon particle and wave behavior, providing a physical explanation for the observed trends. These findings provide valuable insights into phonon transport and offer theoretical support for the development of advanced thermal management strategies.

## 2. Methodology

As shown in the Fig. 1, phonon transport in PGNRs — with width  $W$  and pillar height  $H_p$  — can be interpreted either as particle scattering or wave propagation. Particle scattering within the pillars significantly reduces the phonon mean free path, thereby lowering thermal conductivity. Concurrently, local resonances occur within the pillars, producing standing waves that influence phonon propagation in the surrounding regions. This phenomenon is referred to as resonance hybridization [34].

### 2.1. MC simulation

The MC simulation employed in this study is based on the PBTE, which governs the time evolution of the phonon distribution function  $f(\mathbf{r}, \mathbf{k}, t)$ , where  $\mathbf{r}$  is position,  $\mathbf{k}$  is wave vector, and  $t$  is time. In the absence of external forces, the PBTE is expressed as:

$$\frac{\partial f}{\partial t} + \mathbf{v}_g \cdot \nabla_{\mathbf{r}} f = \left( \frac{\partial f}{\partial t} \right)_{\text{scatter}}, \quad (1)$$

where the phonon group velocity  $\mathbf{v}_g = \nabla_{\mathbf{k}}\omega(\mathbf{k})$  characterizes the rate of phonon energy transport in real space, and the right-hand side describes phonon scattering processes.

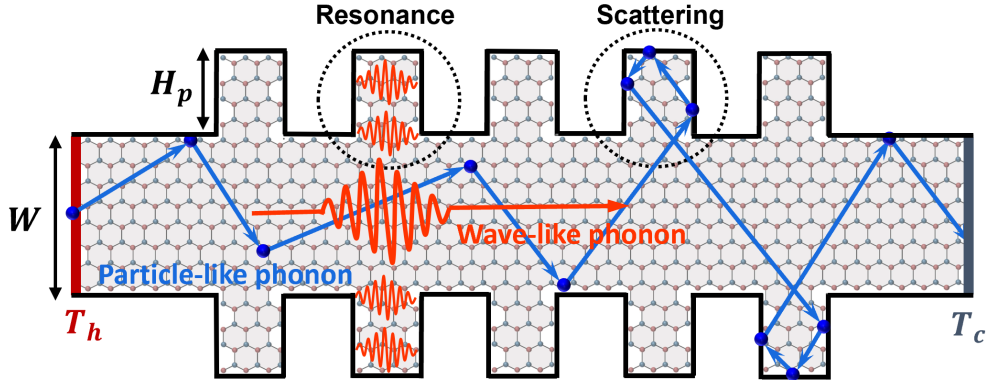


Figure 1: Schematic picture of the phonon transport across PGNR.

Key input information in the phonon MC simulation such as phonon dispersion within the bulk material must be specified. Phonon dispersion is essential for initializing and updating phonon states, including energy and wave vector. The phonon dispersion relation, which defines the relationship between angular frequency and wave vector in the first Brillouin zone, is calculated for graphene using the empirical dynamical matrix method [67–69]. This relation is derived from the secular equation [6]:

$$\omega^2(\mathbf{k})\mathbf{A} = \mathbf{D}(\mathbf{k}) \cdot \mathbf{A}, \quad (2)$$

where  $\omega^2(\mathbf{k})$  is the eigenvalue,  $\mathbf{A}(\mathbf{k})$  is the eigenvector,  $\mathbf{D}(\mathbf{k})$  is the dynamic matrix. The dynamical matrix is constructed via discrete Fourier transformation of the interatomic force constants, using the parameterized 5th-nearest-neighbor force constant (5NNFC) model. The specific parameter values are provided in Table S1 of the Supplementary Material (SM), and further details can be found in Ref. [69]. This approach achieves accuracy on par with first-principles calculations. The input data of our MC simulation has been carefully verified to achieve nearly accurate bulk graphene thermal conductivity [70]. The full phonon dispersion of graphene in the Brillouin zone, is shown in Fig. 2.

In the MC simulation, the left and right boundaries are modeled as isothermal boundaries, represented as black bodies with high temperature  $T_h$  and low temperature  $T_c$ . The upper and lower boundaries, formed by the square-wave-shaped pillars, are treated as reflective boundaries, allowing

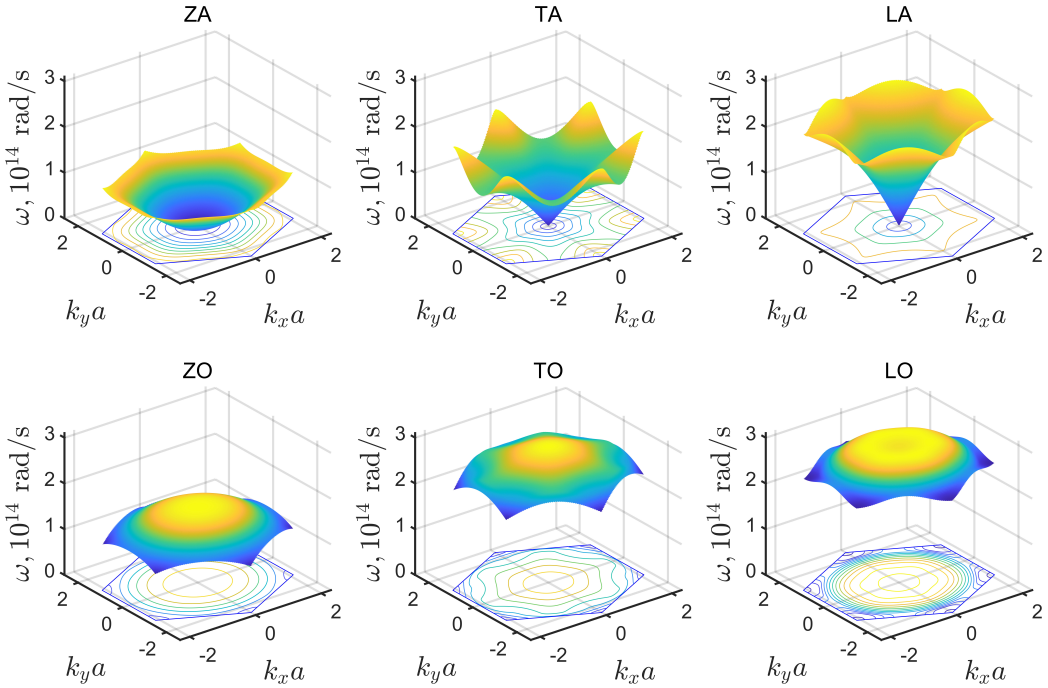


Figure 2: The full dispersion relation of graphene for the ZA, TA, LA, ZO, TO, and LO phonon branches in the Brillouin zone, calculated using the empirical dynamical matrix method with up to 5th-nearest-neighbor interactions.

phonons to elastically scatter off these surfaces, as illustrated in Fig.1. Depending on the boundary roughness, some phonons are specularly reflected, while others undergo diffuse reflection.

Phonon frequencies are determined by matching a random number to the cumulative distribution function (CDF). Once the frequency is established, the phonon mode is selected based on the density of states (DOS) for different modes at that frequency, as depicted in Figs.3a-3c. The CDF after scattering differs from the initial phonon distribution's CDF. A detailed description of the simulation methodology is provided in the SM 2. The flow chart of the MC simulation is presented in Fig.3d. Phonons can travel in two ways: drift or scattering [71–73]. After scattering, energy conservation needs to be achieved by adding or removing phonons.

During the drift step, phonons move ballistically, with their positions updated according to the group velocity  $\vec{r}(t + \Delta t) = \vec{r}(t) + \vec{v}\Delta t$ , where  $\Delta t$  is the time step. For a phonon with frequency  $\omega$  in branch  $j$ , the probability

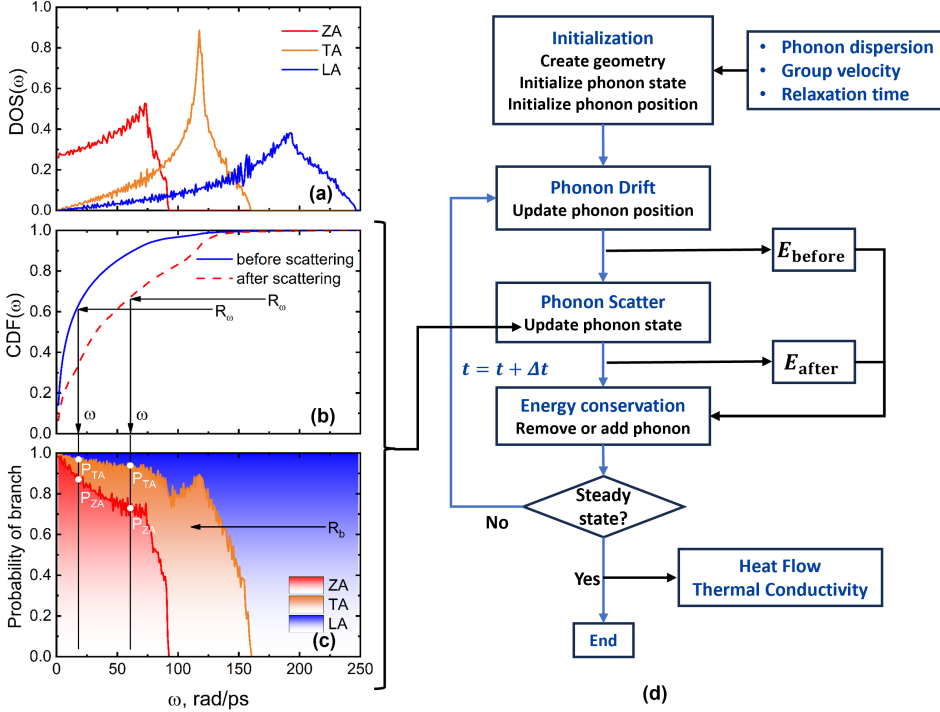


Figure 3: (a) Phonon DOS of ZA, TA and LA branches, (b) CDF before scattering and after scattering, (c) The probability of a phonon with the frequency  $\omega$  being in branch, (d) Flowchart of MC simulation.

of scattering within a time interval  $\Delta t$  is given by:

$$p_j(\omega) = 1 - \exp\left(-\frac{\Delta t}{\tau_j(\omega)}\right), \quad (3)$$

where,  $\tau_j(\omega)$  is the phonon lifetime, representing the inverse of the total scattering rate for a phonon of frequency  $\omega$  in branch  $j$ . This rate is calculated using Fermi's golden rule, which determines the transition probability per unit time due to anharmonic phonon-phonon interactions, including contributions from both normal (N) processes and Umklapp (U) processes.

A random number  $R_{\text{scat}}$  is generated to determine if scattering occurs. If  $R_{\text{scat}} < P_j(\omega)$ , the phonon scatters and is replaced with a new phonon resampled from the CDF after scattering. Once the system reaches steady state, the thermal conductivity is calculated based on the temperature gradient.

In MC simulations, phonons are treated as particles undergoing bound-

ary scattering, which reduces their mean free path and, consequently, the thermal conductivity. MC methods are particularly suited for modeling such particle-like transport phenomena; however, they do not explicitly capture wave-related effects such as coherence, interference, or resonance. As a result, the thermal conductivity values obtained from MC simulations reflect only the reduction due to particle effects. To comprehensively evaluate the influence of wave phenomena—such as phonon resonance hybridization and localization, which can further suppress thermal transport by modifying the wave characteristics of phonons—a comparison with MD simulations is essential.

## 2.2. MD simulation

MD simulations were performed using the LAMMPS software package [74] with an optimized Tersoff potential [75]. The equations of motion were integrated with the velocity Verlet method using a time step of 0.5 fs. Initially, the system was equilibrated under the NPT ensemble (constant number of atoms, pressure, and temperature) at 300 K and 0 bar for 0.5 ns.

Fixed boundary conditions were applied along the x-direction, while periodic boundary conditions were imposed in the y and z directions. A 4 nm vacuum layer was introduced along both the y and z directions to ensure that the system captures the intrinsic properties of monolayer PGNRs. The structure was divided into 80 layers ( $N=80$ ) to establish a stable and well-defined temperature gradient, with atoms in the boundary layers (layers 1–2 and  $N-1$  to  $N$ ) fixed. Langevin thermostats were applied to layers 3–6 and  $N-6$  to  $N-3$  to maintain temperatures of 310 K and 290 K, respectively. The damping parameter of the Langevin thermostat was set to 50 times the simulation time step (25 fs) to maximize the heat flux through the system (see Fig. S1 in SM 3 for details).

The first NVE ensemble (constant number of atoms, volume, and energy) was performed for 2.5 ns to ensure the system was equilibrated in the Langevin hot bath. In the second NVE ensemble, time-averaged values of temperature and heat current were computed over a period of 10 ns. Results represent averages from six independent simulations with varied initial conditions. More details of MD simulation settings can be found in SM 3. The temperature gradient was extracted via linear fitting of the local temperature profile, excluding boundary-induced jumps. Thermal conductivity was

calculated using Fourier's law:

$$\kappa = -\frac{J}{W \cdot d \cdot \nabla T}, \quad (4)$$

where  $J$  is the heat flux,  $d$  is the thickness (0.334 nm), and  $\nabla T$  is the longitudinal temperature gradient. The cross-sectional area used for the RGNR calculation excludes the height of the pillar structures. The temperature  $T_{\text{MD}}$  was determined based on the kinetic energy of the atoms:

$$\frac{3Nk_B T_{\text{MD}}}{2} = \sum_i \frac{m_i v_i^2}{2}. \quad (5)$$

The MD simulations capture the wave-like nature of phonons. A key mechanism in PGNRs is resonance hybridization, which arises when a propagating phonon mode strongly couples with a localized vibrational mode associated with the pillars. This coupling results in band flattening in the dispersion relation, leading to a significant reduction in group velocity near the hybridization region.

### 2.3. Quantitative analysis

For GNRs without pillars, MC and MD simulations yield consistent thermal conductivity results. The key distinction lies in their treatment of boundaries: MD simulations incorporate explicit atomic boundaries, whereas MC simulations rely on statistical boundary conditions. A critical parameter in MC simulations is the specular reflection probability  $p_{\text{spec}}$ , which classical models (e.g., Ziman [76] and Soffer [77]) express as a function of phonon wavelength ( $\lambda$ ), angle of incidence ( $\theta$ ) and boundary roughness ( $\sigma$ ):

$$p_{\text{spec}} = \exp\left(-\frac{16\pi^2\sigma^2}{\lambda^2} \cos^2 \theta\right). \quad (6)$$

By appropriately adjusting  $\sigma$ , MC simulations can replicate the thermal conductivity trends observed in MD simulations for GNRs without pillars. This calibration compensates for the MC method's inherent limitations in capturing atomistic boundary interactions explicitly.

Ensuring agreement between MC and MD results is essential for isolating wave effects—such as resonant hybridization—on phonon transport. Once MC and MD simulations produce similar results for GNRs, any deviations observed in pillared GNRs (PGNRs) can be confidently attributed to wave

effects rather than methodological differences [27, 78]. This alignment provides a solid foundation for analyzing the interplay between particle-like and wave-like phonon transport mechanisms in nanostructured materials. (Detailed calibration process is provided in the SM 5.)

We employed MC simulations to calculate the thermal conductivities of both GNR and PGNR, denoted as  $\kappa_{\text{GNR}}^{\text{MC}}$  and  $\kappa_{\text{PGNR}}^{\text{MC}}$ , respectively, and MD simulations to determine the thermal conductivities of both GNR and PGNR, represented as  $\kappa_{\text{GNR}}^{\text{MD}}$  and  $\kappa_{\text{PGNR}}^{\text{MD}}$ , respectively. Here,  $\kappa_{\text{GNR}}^{\text{MC}} = \kappa_{\text{GNR}}^{\text{MD}} = \kappa_{\text{GNR}}$  is used as the benchmark for comparison.

To facilitate this, we define the relative thermal conductivities as:

$$\kappa_{\text{rel}}^{\text{MC}} = \frac{\kappa_{\text{PGNR}}^{\text{MC}}}{\kappa_{\text{GNR}}}, \quad \kappa_{\text{rel}}^{\text{MD}} = \frac{\kappa_{\text{PGNR}}^{\text{MD}}}{\kappa_{\text{GNR}}}. \quad (7)$$

These relative thermal conductivities represent the ratios of the thermal conductivity of PGNR to the thermal conductivity of GNR.

To quantitatively distinguish the phonon particle and wave effects more clearly, we define the wave ratio,  $\eta_{\text{wave}}$ , which represents the proportion of reduction in thermal conductivity attributed to the wave effects relative to the total reduction in thermal conductivity. This ratio is expressed as follows:

$$\eta_{\text{wave}} = \frac{\kappa_{\text{PGNR}}^{\text{MC}} - \kappa_{\text{PGNR}}^{\text{MD}}}{\kappa_{\text{GNR}} - \kappa_{\text{PGNR}}^{\text{MD}}} = \frac{\kappa_{\text{rel}}^{\text{MC}} - \kappa_{\text{rel}}^{\text{MD}}}{1 - \kappa_{\text{rel}}^{\text{MD}}}. \quad (8)$$

The particle ratio is then defined as:

$$\eta_{\text{particle}} = 1 - \eta_{\text{wave}}. \quad (9)$$

### 3. Results and Discussion

The Debye temperatures of graphene, GNRs, and PGNRs were estimated based on the average phonon group velocity, yielding 1593 K for graphene, 445 K for GNRs, and 306 K for PGNRs. The derivation of the Debye temperature and its validation via comparison with literature values are provided in SM 4. The method follows the approaches described in Refs. [79, 80], and the calculated results are summarized in tabular form. Consequently, the investigation of thermal conductivity variations with size was conducted at room temperature (300 K).

Fig. 4a and Fig. 4b show the thermal conductivity of GNRs and PGNRs as functions of width  $W$  (pillar height  $H_p$  fixed at 0.86 nm) and pillar height

$H_p$  (width  $W$  fixed at 1.72 nm), respectively. Fig. 4d and Fig. 4e present the relative thermal conductivity under the same conditions. Fig. 4g and Fig. 4h depict the wave ratio (proportion of wave effects in thermal conductivity reduction) as functions of  $W$  and  $H_p$ , respectively. Simulations were performed for GNRs ( $W$ : 1.72 nm) and PGNRs ( $W$ : 1.72 nm,  $H_p$ : 0.86 nm) across a range of temperatures, with the corresponding results shown in Fig. 4c, 4f, and 4i.

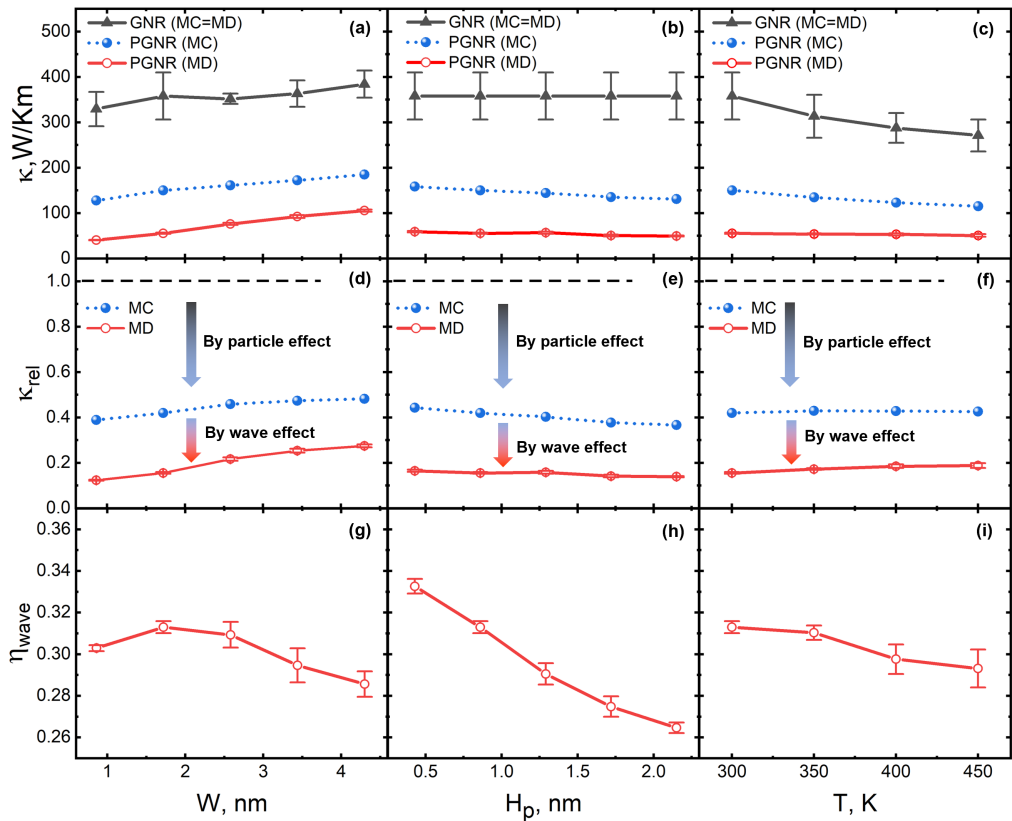


Figure 4: (a)-(c) Thermal conductivity of GNR and PGNR obtained from MC and MD simulations: (a) vs. width  $W$  ( $H_p = 0.86$  nm,  $T = 300$  K); (b) vs. pillar height  $H_p$  ( $W = 1.72$  nm,  $T = 300$  K); (c) vs. temperature  $T$  ( $W = 1.72$  nm,  $H_p = 0.86$  nm). (d)-(f) Relative thermal conductivity of PGNR: (d) vs. width  $W$ ; (e) vs. vs. pillar height  $H_p$ ; (f) vs. temperature  $T$  (same conditions as (a)-(c)). (g)-(i) Wave ratio of PGNR: (g) vs. width  $W$ ; (h) vs. pillar height  $H_p$ ; (i) vs. temperature  $T$  (same conditions as (a)-(c)).

Fig. 4a, Fig. 4b and Fig. 4c reveal variations in the thermal conductivity of PGNRs with width  $W$ , pillar height  $H_p$  and temperature  $T$ , as

determined by MC and MD simulations. These discrepancies arise from the computational approaches: MC simulations focus solely on particle effects, where scattering in pillar reduces the mean free path of particles. In contrast, MD simulations account for both particle and wave effects, including local resonances or standing waves at the pillars, which influence heat transport at the nanoscale. Comparing MC and MD results highlights the distinct contributions of wave and particle effects.

Fig. 4d, Fig. 4e and Fig. 4f show how relative thermal conductivity changes with width  $W$ , pillar height  $H_p$  and temperature  $T$ . The horizontal line represents a relative thermal conductivity of 1. The reduction from this line to the blue dashed line reflects particle effects, while the further reduction to the red solid line indicates wave effects. Particle effects cause a larger reduction in thermal conductivity compared to wave effects.

Our results indicate that particle effects lead to a greater reduction in thermal conductivity than wave effects. This behavior contrasts with that observed in silicon nanowires, where wave effects are dominant [31]. The discrepancy can be attributed to the intrinsically high thermal conductivity of graphene and the exceptionally long phonon mean free path. In PGNRs, phonon transport is highly sensitive to boundary scattering. Particle effects substantially shorten the phonon mean free path, leading to a pronounced decrease in thermal conductivity.

Furthermore, the dimensionality of the systems contributes to this difference. Silicon nanowires are quasi-one-dimensional structures embedded in three-dimensional space, while PGNRs are quasi-one-dimensional in a two-dimensional plane. The latter supports fewer phonon modes, reducing the likelihood of resonance hybridization. This structural difference explains why wave effects are more prominent in silicon nanowires than in PGNRs.

Consistent with earlier studies, our results also show that wave effects diminish as system size increases. For instance, [27] demonstrated that the thermal conductivity of pristine graphene increases monotonically with length in both MD simulations and PBTE calculations, with good agreement between the two approaches. However, in nanoporous graphene, wave effects weaken as the structure becomes larger. This is because wave-like behavior is intrinsically linked to the phonon wavelength. When the characteristic dimensions of the system greatly exceed the dominant phonon wavelengths, phonon transport can be effectively described using a classical particle-based model.

To highlight the influence of particle effects on the thermal conductivity

of the structure, a graph of phonon trajectories was generated (Fig. 5a). This phonon path diagram from the MC simulation clearly demonstrates that the presence of pillars enhances phonon boundary scattering, leading to a substantial reduction in the phonon mean free path and, consequently, the thermal conductivity. As the pillar height  $H_p$  increases, this effect intensifies, as a larger fraction of phonons undergo boundary scattering within the pillars, thereby amplifying the contribution of particle effects. Fig. 5b shows the ratio ( $l_{\text{PGNR}}/l_{\text{GNR}}$ ) of the phonon mean free path (MFP) in PGNRs to that in pristine GNRs as a function of width  $W$  and pillar height  $H_p$ . For the black curve, the  $H_p$  is fixed at 0.86 nm while the  $W$  varies; for the blue curve, the  $W$  is fixed at 1.72 nm while the  $H_p$  varies. The results demonstrate that increasing  $H_p$  or decreasing  $W$  leads to a lower MFP ratio, indicating enhanced boundary scattering and reduced transport efficiency due to dominant particle effects.

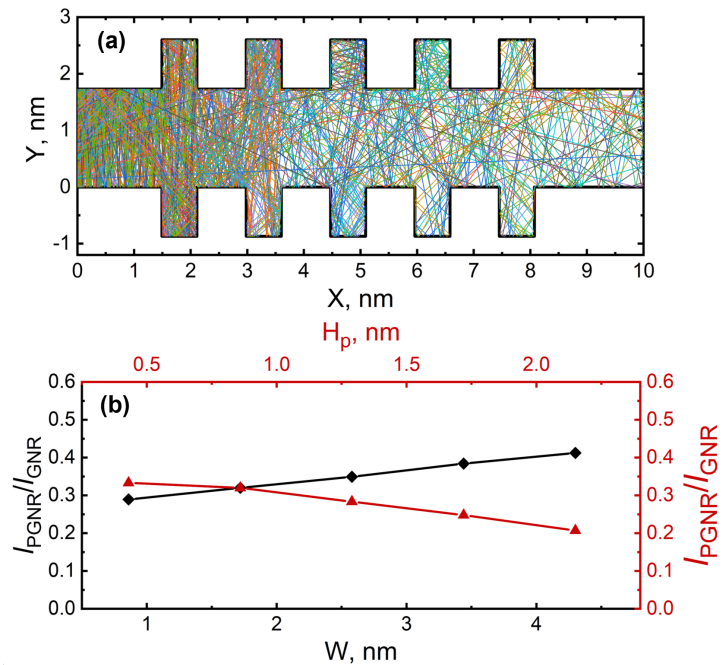


Figure 5: (a) Particle effect mechanism: scattering with boundaries leads to a reduction in the mean free path of phonons in MC simulation. (b) The ratio of the phonon mean free path in PGNR to that in GNR as a function of width  $W$  and pillar height  $H_p$ . In the case of varying  $W$ , the  $H_p$  is fixed at 0.86 nm (black curve); in the case of varying  $H_p$ , the  $W$  is fixed at 1.72 nm (red curve).

Phonon resonance and localization within PGNRs are key indicators of wave effects, which also contribute to reduced thermal conductivity. When the resonance frequency of a pillar interferes with the primary phonon frequency, phonon transport within the pillar is suppressed, and nearby phonons in the main structure are also affected. These phonons exhibit resonant hybrid modes, resulting in a reduced phonon group velocity, as shown in Fig. 6a and 6b, where the presence of the pillar causes a significant decrease in the group velocity to decrease by a factor of three. This significant reduction in group velocity further diminishes the thermal conductivity.

The thermal conductivity of PGNRs decreases with increasing pillar height  $H_p$  for several reasons. First, a greater  $H_p$  introduces a larger number of resonant modes, which significantly enhances phonon scattering, thereby reducing thermal conductivity [30]. Second, taller pillars induce resonant modes at lower frequencies [34], leading to increased hybridization in the low-frequency range, which contributes more strongly to thermal transport in low-dimensional systems. This enhanced hybridization disrupts coherent phonon transport and further suppresses thermal conductivity. Moreover, our observation is consistent with previously reported results for nanowires with surface pillars, reinforcing the validity of this interpretation [81].

In Fig. 4f, the relative thermal conductivity of PGNRs calculated via MD ( $\kappa_{\text{rel}}^{\text{MD}}$ ) exhibits a slight upward trend. Here,  $\kappa_{\text{rel}}^{\text{MD}}$  is defined as the ratio  $\kappa_{\text{PGNR}}^{\text{MD}}/\kappa_{\text{GNR}}^{\text{MD}}$ . Although both  $\kappa_{\text{PGNR}}^{\text{MD}}$  and  $\kappa_{\text{GNR}}^{\text{MD}}$  decrease with increasing temperature due to enhanced phonon–phonon scattering (see Fig. 4c), the scattering in PGNRs is significantly stronger. As a result, the thermal conductivity of PGNRs decreases more gradually with temperature, leading to a slight increase in  $\kappa_{\text{rel}}^{\text{MD}}$  as temperature rises. From Fig. 4i, it can also be observed that in the medium and low temperature regions, the wave ratio decreases slightly with increasing temperature. This is attributed to two effects: shorter phonon wavelengths at higher temperatures and increased scattering events, both of which undermine the coherence necessary for wave-like phonon transport.

Fig. 4g shows that the wave ratio initially increases and then decreases as the PGNR width  $W$  decreases. This trend occurs because the contribution of phonon wave effects reaches saturation as the  $W$  decreases. Once saturated, the wave effect contribution no longer increases, while pillar scattering and boundary scattering continue to play a larger role in reducing thermal conductivity as the  $W$  decreases.

As the  $W$  of PGNR increases, the wave ratio will eventually decrease,

which is consistent with previous studies that the wave effects will decrease with the increase in size, and for materials with large sizes, the wave effects can be ignored [31]. As shown in Fig. 4h, as the Pillar height  $H_p$  increases, the wave ratio will decrease monotonically, because the proportion of phonons scattered in the pillar is increasing, which will lead to a significant decrease in thermal conductivity and a relative decrease in the ratio of the wave effect. As shown in Fig. 4i, the wave ratio decreases as the temperature rises. This is due to the enhanced particle scattering at higher temperatures, which disrupts wave effects.

The dispersion relations of phonons in GNR and PGNR are presented in Fig. 6a, with the resonance hybridization modes indicated. The group velocity of PGNR is effectively decreased by resonance hybridization (Fig. 6b). And the product of group velocity and DOS (Fig. 6c) is closely related to the thermal conductivity. The integral of the product is calculated, and the ratio ( $R$ ) of the integral can show the decrease of group velocity by resonance hybridization as

$$R = \frac{\int \bar{v}_g^{\text{PGNR}}(\omega) \cdot \text{dos}(\omega) d\omega}{\int \bar{v}_g^{\text{GNR}}(\omega) \cdot \text{dos}(\omega) d\omega}. \quad (10)$$

The dependence of  $R$  on the width of PGNR ( $W$ ) is shown in Fig. 6d. The values of  $R$  decrease with the width for three structures with different pillar height. The data is well-fitted by the sigmoid-like function:

$$R(W) = \frac{a}{1 + \exp[-b(W - c)]} + 1 - a, \quad (11)$$

which satisfies the condition  $\lim_{x \rightarrow \infty} R(W) = 1$ , reflecting the convergence of PGNR behavior to that of GNRs at large widths. In Eq. (11), the value of  $c$  corresponds to the point at which the growth rate of  $R$  is maximal (i.e., the steepest slope, as shown in Fig. S7 in SM 7). The parameter  $b$  shows the sharpness of the transition, for example a larger value of  $b$  means a steeper and narrower peak, indicating a more abrupt change in group velocity behavior.

As shown in Fig. 6d, there is a characteristic value,  $c - 1/b$ , which corresponds to the point where  $R$  begins to decrease slowly, signaling start of the overlapping of two hybridization areas (see the middle structure in Fig. 6e). That is, the width of PGNR is close to two times of resonance hybridization depth. Then, the resonance hybridization depth ( $D$ ) is

$$D = (c - 1/b)/2, \quad (12)$$

representing the spatial extent over which hybridization significantly modifies the transport of phonons.

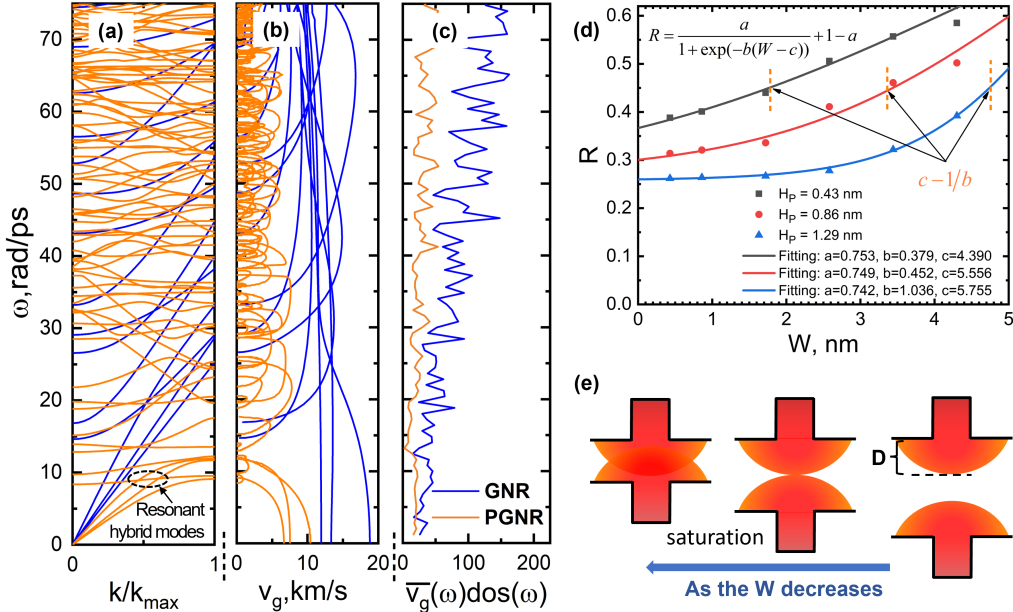


Figure 6: (a) Dispersion relations of phonons in GNR and PGNR. (b) Group velocity comparison between GNR and PGNR, showing reduction in PGNR by resonance hybridization. (c) The product of group velocity and DOS of phonons in GNR and PGNR. (d) The ratio ( $R$ ) of the integral of the product versus PGNR width for various pillar heights. (e) Schematic of resonance hybridization depth in PGNR structures.

For PGNRs with pillar heights  $H_p = 0.43$  nm,  $H_p = 0.86$  nm and  $H_p = 1.29$  nm, the corresponding resonance hybridization depths are approximately  $D = 0.87$  nm,  $D = 1.67$  nm and  $D = 2.40$  nm, respectively (see Fig.6d). These findings demonstrate that taller pillars result in deeper resonance hybridization, consistent with the expectation that stronger local resonances induce broader spatial modulation of phonon modes.

This analysis confirms that the resonance hybridization depth is not a universal constant but instead varies with structural parameters such as pillar height.

The quantitative analysis of particle and wave effects provides a framework for understanding how structural design influences thermal transport in PGNRs. Identifying the dominant transport mechanism under specific ge-

ometries enables the targeted optimization of pillar height  $H_p$  and periodicity. This insight supports the design of thermal rectifiers with directional heat flow and thermal management devices with tailored conductivity for efficient heat dissipation. Specifically, particle effects can be harnessed to enhance ballistic transport in short channels, while wave effects can be exploited to engineer interference-based thermal barriers or filters.

#### 4. Conclusion

This study quantitatively analyzed the respective roles of particle and wave effects in phonon transport within pillared graphene nanoribbons (PGNRs) by comparing Monte Carlo (MC) and molecular dynamics (MD) simulations. The MC results demonstrate that the introduction of pillars significantly enhances phonon-boundary scattering, leading to a reduction in thermal conductivity. In contrast, the MD simulations, which inherently capture both particle and wave phenomena, reveal a more nuanced interplay between scattering and resonance effects.

Our findings suggest that particle-like behavior plays a dominant role in thermal transport suppression in graphene-based nanostructures. This trend may be attributed to two key factors: (1) the intrinsically long phonon mean free path in graphene renders heat transport particularly sensitive to boundary scattering, and (2) the reduced dimensionality of PGNRs limits the available phonon modes, thereby decreasing the likelihood of strong resonance hybridization. While these insights are supported by our simulations, a more comprehensive understanding requires further investigation across a broader range of material systems and structural configurations.

Future work will focus on evaluating the universality of the proposed resonance hybridization depth as a metric for characterizing wave effects in various pillared nanostructures. Additionally, we will examine the influence of structural imperfections and temperature variations on phonon transport and resonance behavior, aiming to deepen the understanding of thermal stability and scattering mechanisms in low-dimensional materials.

#### CRediT authorship contribution statement

**S. Liu:** Methodology, Validation, Formal analysis, Investigation, Writing - original draft, Writing - review & editing. **Z. Zong:** Methodology, Validation, Formal analysis, Investigation, Writing - review & editing. **F. Yin:**

Validation, Formal analysis, Writing - review & editing. **V.I. Khvesyuk:** Conceptualization, Supervision, Writing - review & editing. **N. Yang:** Conceptualization, Methodology, Supervision, Writing - review & editing.

### Declaration of Competing Interest

The authors declare that they have no known competing financial interests or personal relationships that could have appeared to influence the work reported in this paper.

### Acknowledgements

The work was carried out at the National Supercomputer Center in Tianjin, and the calculations were performed on TianHe-HPC. S. Liu and F. Yin gratefully acknowledges financial support from the China Scholarship Council (No. 202308090243 for S. Liu and No. 202408090635 for F. Yin). The authors sincerely thank Shiyun Xiong, Lina Yang, Dengke Ma and A.A. Barinov for their valuable discussions and insightful suggestions.

### Appendix A. Summary of Supplementary Material

The SM provides additional computational and methodological details supporting this work:

SM 1 describes the construction of graphene's phonon dispersion using the empirical fifth-nearest-neighbor force constant (5NNFC) model, with the corresponding force constants listed in Table S1.

SM 2 outlines the Monte Carlo (MC) simulation procedure, including phonon initialization, drift, scattering, and thermal conductivity calculation.

SM 3 presents the setup of non-equilibrium molecular dynamics (NEMD) simulations using the optimized Tersoff potential within the LAMMPS package.

SM 4 explains the estimation of the Debye temperature based on phonon group velocities and integration over the phonon density of states (DOS).

SM 5 details the calibration of boundary roughness  $\sigma$  in MC simulations using the Ziman-Soffer model to account for wavelength-dependent specular-ity.

SM 6 clarifies that the PGNR width refers to the width of the GNR base structure, excluding the height of the pillars.

SM 7 illustrates the properties of the fitting function via graphical representations.

## References

- [1] S. Datta, Electronic Transport in Mesoscopic Systems, Cambridge Studies in Semiconductor Physics and Microelectronic Engineering, Cambridge University Press, Cambridge, 1995. doi:10.1017/CBO9780511805776.
- [2] C. Heide, T. Higuchi, H. B. Weber, P. Hommelhoff, Coherent Electron Trajectory Control in Graphene, *Phys. Rev. Lett.* 121 (20) (2018) 207401. doi:10.1103/PhysRevLett.121.207401.
- [3] N. K. Langford, S. Ramelow, R. Prevedel, W. J. Munro, G. J. Milburn, A. Zeilinger, Efficient quantum computing using coherent photon conversion, *Nature* 478 (7369) (2011) 360–363. doi:10.1038/nature10463.
- [4] K. Konthasinghe, J. Walker, M. Peiris, C. K. Shih, Y. Yu, M. F. Li, J. F. He, L. J. Wang, H. Q. Ni, Z. C. Niu, A. Muller, Coherent versus incoherent light scattering from a quantum dot, *Phys. Rev. B* 85 (23) (2012) 235315. doi:10.1103/PhysRevB.85.235315.
- [5] M. N. Luckyanova, J. Garg, K. Esfarjani, A. Jndl, M. T. Bulsara, A. J. Schmidt, A. J. Minnich, S. Chen, M. S. Dresselhaus, Z. Ren, E. A. Fitzgerald, G. Chen, Coherent Phonon Heat Conduction in Superlattices, *Science* 338 (6109) (2012) 936–939. doi:10.1126/science.1225549.
- [6] G. P. Srivastava, The Physics of Phonons, 2nd Edition, CRC Press, Boca Raton, 2022. doi:10.1201/9781003141273.
- [7] D. G. Cahill, W. K. Ford, K. E. Goodson, G. D. Mahan, A. Majumdar, H. J. Maris, R. Merlin, S. R. Phillpot, Nanoscale thermal transport, *Journal of Applied Physics* 93 (2) (2003) 793–818. doi:10.1063/1.1524305.
- [8] E. Pop, Energy dissipation and transport in nanoscale devices, *Nano Res.* 3 (3) (2010) 147–169. doi:10.1007/s12274-010-1019-z.

- [9] S. K. Gupta, S. Gupta, The role of nanofluids in solar thermal energy: A review of recent advances, *Materials Today: Proceedings* 44 (2021) 401–412.
- [10] S. K. Gupta, S. Dixit, Progress and application of nanofluids in solar collectors: An overview of recent advances, *Materials Today: Proceedings* 44 (2021) 250–259.
- [11] S. K. Gupta, A. Sharma, A brief review of nanofluids utilization in heat transfer devices for energy saving, *Materials Today: Proceedings* (2023).
- [12] C. W. Chang, D. Okawa, A. Majumdar, A. Zettl, Solid-State Thermal Rectifier, *Science* 314 (5802) (2006) 1121–1124. doi:10.1126/science.1132898.
- [13] N. Yang, G. Zhang, B. Li, Carbon nanocone: A promising thermal rectifier, *Applied Physics Letters* 93 (24) (2008) 243111. doi:10.1063/1.3049603.
- [14] G. J. Snyder, E. S. Toberer, Complex thermoelectric materials, *Nature Mater* 7 (2) (2008) 105–114. doi:10.1038/nmat2090.
- [15] M. S. Dresselhaus, G. Chen, M. Y. Tang, R. G. Yang, H. Lee, D. Z. Wang, Z. F. Ren, J.-P. Fleurial, P. Gogna, New Directions for Low-Dimensional Thermoelectric Materials, *Advanced Materials* 19 (8) (2007) 1043–1053. doi:10.1002/adma.200600527.
- [16] X.-K. Chen, E.-M. Zhang, D. Wu, K.-Q. Chen, Strain-induced medium-temperature thermoelectric performance of  $\text{Cu}_4\text{TiSe}_4$ : The role of four-phonon scattering, *Phys. Rev. Appl.* 19 (2023) 044052. doi:10.1103/PhysRevApplied.19.044052.  
URL <https://link.aps.org/doi/10.1103/PhysRevApplied.19.044052>
- [17] S. Liu, A. A. Barinov, F. Yin, V. I. Khvesyuk, Determination of thermal properties of unsmooth Si-nanowires, *Chinese Phys. Lett.* 41 (2024) 016301.
- [18] J. Lim, K. Hippalgaonkar, S. C. Andrews, A. Majumdar, P. Yang, Quantifying Surface Roughness Effects on Phonon Transport in Silicon Nanowires, *Nano Lett* 12 (5) (2012) 2475–2482. doi:10.1021/nl3005868.

- [19] H.-Y. Yang, Y.-L. Chen, W.-X. Zhou, G.-F. Xie, N. Xu, Ultra-low thermal conductivity of roughened silicon nanowires: Role of phonon-surface bond order imperfection scattering\*, Chinese Phys. B 29 (8) (2020) 086502. doi:10.1088/1674-1056/ab99af.
- [20] C.-D. Zhou, B. Liang, W.-J. Huang, J.-G. Noudem, X.-J. Tan, J. Jiang, Phonon engineering significantly reducing thermal conductivity of thermoelectric materials: A review, Rare Met. 42 (9) (2023) 2825–2839. doi:10.1007/s12598-023-02302-3.
- [21] W. Lang, A. Drost, P. Steiner, H. Sandmaier, The Thermal Conductivity of Porous Silicon, MRS Proc. 358 (1994) 561. doi:10.1557/PROC-358-561.
- [22] M. N. Esfahani, M. Jabbari, Y. Xu, C. Soutis, Effect of nanoscale defects on the thermal conductivity of graphene, Materials Today Communications 26 (2021) 101856. doi:10.1016/j.mtcomm.2020.101856.
- [23] N. Yang, G. Zhang, B. Li, Ultralow Thermal Conductivity of Isotope-Doped Silicon Nanowires, Nano Lett. 8 (1) (2008) 276–280. doi:10.1021/nl0725998.
- [24] Z. Zhang, Y. Guo, M. Bescond, J. Chen, M. Nomura, S. Volz, Heat Conduction Theory Including Phonon Coherence, Phys. Rev. Lett. 128 (1) (2022) 015901. doi:10.1103/PhysRevLett.128.015901.
- [25] G. Xie, D. Ding, G. Zhang, Phonon coherence and its effect on thermal conductivity of nanostructures, Advances in Physics: X 3 (1) (2018) 1480417. doi:10.1080/23746149.2018.1480417.
- [26] B. Latour, S. Volz, Y. Chalopin, Microscopic description of thermal-phonon coherence: From coherent transport to diffuse interface scattering in superlattices, Phys. Rev. B 90 (1) (2014) 014307. doi:10.1103/PhysRevB.90.014307.
- [27] H. Wei, Y. Hu, H. Bao, X. Ruan, Quantifying the diverse wave effects in thermal transport of nanoporous graphene, Carbon 197 (2022) 18–26. doi:10.1016/j.carbon.2022.06.011.
- [28] S. Hu, Z. Zhang, P. Jiang, J. Chen, S. Volz, M. Nomura, B. Li, Randomness-Induced Phonon Localization in Graphene Heat

Conduction, J. Phys. Chem. Lett. 9 (14) (2018) 3959–3968.  
doi:10.1021/acs.jpclett.8b01653.

- [29] B. L. Davis, M. I. Hussein, Nanophononic Metamaterial: Thermal Conductivity Reduction by Local Resonance, Phys. Rev. Lett. 112 (5) (2014) 055505. doi:10.1103/PhysRevLett.112.055505.
- [30] D. Ma, X. Wan, N. Yang, Unexpected thermal conductivity enhancement in pillared graphene nanoribbon with isotopic resonance, Phys. Rev. B 98 (24) (2018) 245420. doi:10.1103/PhysRevB.98.245420.
- [31] D. Ma, A. Arora, S. Deng, G. Xie, J. Shiomi, N. Yang, Quantifying phonon particle and wave transport in silicon nanophononic metamaterial with cross junction, Materials Today Physics 8 (2019) 56–61. doi:10.1016/j.mtphys.2019.01.002.
- [32] S. Tian, T. Wang, H. Chen, D. Ma, L. Zhang, Phonon coherent transport leads to an anomalous boundary effect on the thermal conductivity of a rough graphene nanoribbon, Phys. Rev. Applied 21 (6) (2024) 064005. doi:10.1103/PhysRevApplied.21.064005.
- [33] G. Qin, X. Zhang, S.-Y. Yue, Z. Qin, H. Wang, Y. Han, M. Hu, Resonant bonding driven giant phonon anharmonicity and low thermal conductivity of phosphorene, Phys. Rev. B 94 (16) (2016) 165445. doi:10.1103/PhysRevB.94.165445.
- [34] S. Xiong, K. Sääskilahti, Y. A. Kosevich, H. Han, D. Donadio, S. Volz, Blocking Phonon Transport by Structural Resonances in Alloy-Based Nanophononic Metamaterials Leads to Ultralow Thermal Conductivity, Phys. Rev. Lett. 117 (2) (2016) 025503. doi:10.1103/PhysRevLett.117.025503.
- [35] K. Li, Y. Cheng, H. Wang, Y. Guo, Z. Zhang, M. Bescond, M. Nomura, S. Volz, X. Zhang, S. Xiong, Phonon resonant effect in silicon membranes with different crystallographic orientations, International Journal of Heat and Mass Transfer 183 (2022) 122144. doi:10.1016/j.ijheatmasstransfer.2021.122144.
- [36] L. Yang, Y. Xu, X. Wang, Y. Zhou, Tuning the thermal conductivity of a silicon membrane using nanopillars: From crystalline

to amorphous pillars, Phys. Rev. Applied 22 (3) (2024) 034016. doi:10.1103/PhysRevApplied.22.034016.

- [37] W.-X. Zhou, Y. Cheng, K.-Q. Chen, G. Xie, T. Wang, G. Zhang, Thermal Conductivity of Amorphous Materials, Adv Funct Materials 30 (8) (2020) 1903829. doi:10.1002/adfm.201903829.
- [38] X. Li, X. Wang, L. Zhang, S. Lee, H. Dai, Chemically Derived, Ultrasmooth Graphene Nanoribbon Semiconductors, Science 319 (5867) (2008) 1229–1232. doi:10.1126/science.1150878.
- [39] T. Radsar, H. Khalesi, V. Ghods, Graphene nanoribbon field effect transistors analysis and applications, Superlattices and Microstructures 153 (2021) 106869. doi:10.1016/j.spmi.2021.106869.
- [40] J. Kusuma, R. G. Balakrishna, S. Patil, M. S. Jyothi, H. R. Chandan, R. Shwetharani, Exploration of graphene oxide nanoribbons as excellent electron conducting network for third generation solar cells, Solar Energy Materials and Solar Cells 183 (2018) 211–219. doi:10.1016/j.solmat.2018.01.039.
- [41] H. Wang, H. S. Wang, C. Ma, L. Chen, C. Jiang, C. Chen, X. Xie, A.-P. Li, X. Wang, Graphene nanoribbons for quantum electronics, Nat Rev Phys 3 (12) (2021) 791–802. doi:10.1038/s42254-021-00370-x.
- [42] Y.-W. Son, M. L. Cohen, S. G. Louie, Half-metallic graphene nanoribbons, Nature 444 (7117) (2006) 347–349. doi:10.1038/nature05180.
- [43] M. Y. Han, B. Özyilmaz, Y. Zhang, P. Kim, Energy Band-Gap Engineering of Graphene Nanoribbons, Phys. Rev. Lett. 98 (20) (2007) 206805. doi:10.1103/PhysRevLett.98.206805.
- [44] A. K. Majee, Z. Aksamija, Length divergence of the lattice thermal conductivity in suspended graphene nanoribbons, Phys. Rev. B 93 (23) (2016) 235423. doi:10.1103/PhysRevB.93.235423.
- [45] F. Mazzamuto, J. Saint-Martin, A. Valentin, C. Chassat, P. Dollfus, Edge shape effect on vibrational modes in graphene nanoribbons: A numerical study, Journal of Applied Physics 109 (6) (2011) 064516. doi:10.1063/1.3552293.

- [46] A. V. Savin, Y. S. Kivshar, Vibrational Tamm states at the edges of graphene nanoribbons, *Phys. Rev. B* 81 (16) (2010) 165418. doi:10.1103/PhysRevB.81.165418.
- [47] S. Mei, L. N. Maurer, Z. Aksamija, I. Knezevic, Full-dispersion Monte Carlo simulation of phonon transport in micron-sized graphene nanoribbons, *Journal of Applied Physics* 116 (16) (2014) 164307. doi:10.1063/1.4899235.
- [48] L. Cui, G. Wei, Z. Li, J. Ma, X. Du, Coherent and incoherent effects of nanopores on thermal conductance in silicene, *International Journal of Thermal Sciences* 167 (2021) 107009. doi:10.1016/j.ijthermalsci.2021.107009.
- [49] X. Wan, D. Ma, D. Pan, L. Yang, N. Yang, Optimizing thermal transport in graphene nanoribbon based on phonon resonance hybridization, *Materials Today Physics* 20 (2021) 100445. doi:10.1016/j.mtphys.2021.100445.
- [50] Y. Wang, B. Qiu, X. Ruan, Edge effect on thermal transport in graphene nanoribbons: A phonon localization mechanism beyond edge roughness scattering, *Applied Physics Letters* 101 (1) (2012) 013101. doi:10.1063/1.4732155.
- [51] X. Wan, D. Pan, Z. Zong, Y. Qin, J.-T. Lü, S. Volz, L. Zhang, N. Yang, Modulating Thermal Conductivity via Targeted Phonon Excitation, *Nano Lett.* 24 (23) (2024) 6889–6896. doi:10.1021/acs.nanolett.4c00478.
- [52] J. Callaway, Model for Lattice Thermal Conductivity at Low Temperatures, *Physical Review* 113 (4) (1959) 1046–1051. doi:10.1103/PhysRev.113.1046.
- [53] M. G. Holland, Analysis of Lattice Thermal Conductivity, *Physical Review* 132 (6) (1963) 2461–2471. doi:10.1103/PhysRev.132.2461.
- [54] P. Giannozzi, S. Baroni, N. Bonini, M. Calandra, R. Car, C. Cavazzoni, D. Ceresoli, G. L. Chiarotti, M. Cococcioni, I. Dabo, et al., Quantum espresso: a modular and open-source software project for quantum simulations of materials, *Journal of physics: Condensed matter* 21 (39) (2009) 395502.

- [55] P. Giannozzi, O. Andreussi, T. Brumme, O. Bunau, M. B. Nardelli, M. Calandra, R. Car, C. Cavazzoni, D. Ceresoli, M. Cococcioni, et al., Advanced capabilities for materials modelling with quantum espresso, *Journal of physics: Condensed matter* 29 (46) (2017) 465901.
- [56] S. T. R. Rizvi, S. U.-D. Khan, M. Hassan, I. Fatima, S. U.-D. Khan, Stable propagation of optical solitons for nonlinear Schrödinger equation with dispersion and self phase modulation, *Mathematics and Computers in Simulation* 179 (2021) 126–136. doi:10.1016/j.matcom.2020.08.014.
- [57] M. Omini, A. Sparavigna, An iterative approach to the phonon Boltzmann equation in the theory of thermal conductivity, *Physica B: Condensed Matter* 212 (2) (1995) 101–112. doi:10.1016/0921-4526(95)00016-3.
- [58] A. Ward, D. A. Broido, D. A. Stewart, G. Deinzer, *Ab initio* theory of the lattice thermal conductivity in diamond, *Physical Review B* 80 (12) (2009) 125203. doi:10.1103/PhysRevB.80.125203.
- [59] W. Li, J. Carrete, N. A. Katcho, N. Mingo, ShengBTE: A solver of the Boltzmann transport equation for phonons, *Computer Physics Communications* 185 (6) (2014) 1747–1758. doi:10.1016/j.cpc.2014.02.015.
- [60] A. Togo, First-principles Phonon Calculations with Phonopy and Phono3py, *Journal of the Physical Society of Japan* 92 (1) (2023) 012001. doi:10.7566/JPSJ.92.012001.
- [61] Y. Hu, R. Jia, J. Xu, Y. Sheng, M. Wen, J. Lin, Y. Shen, H. Bao, Giftbte: an efficient deterministic solver for non-gray phonon boltzmann transport equation, *Journal of Physics: Condensed Matter* 36 (2) (2023) 025901.
- [62] R. Jia, Y. Sheng, J. Xu, H. Xie, H. Bao, The effective thermal conductivity of micro/nanofilm under different heating conditions using nongray Boltzmann transport equation, *International Journal of Thermal Sciences* 208 (2025) 109446. doi:10.1016/j.ijthermalsci.2024.109446.
- [63] J. Hu, S. Schiffli, A. Vallabhaneni, X. Ruan, Y. P. Chen, Tuning the thermal conductivity of graphene nanoribbons by edge passivation and isotope engineering: A molecular dynamics study, *Applied Physics Letters* 97 (13) (2010) 133107. arXiv:1008.1288, doi:10.1063/1.3491267.

- [64] Z. Guo, D. Zhang, X.-G. Gong, Thermal conductivity of graphene nanoribbons, *Applied Physics Letters* 95 (16) (2009) 163103. doi:10.1063/1.3246155.
- [65] R. Anufriev, D. Ohori, Y. Wu, R. Yanagisawa, L. Jalabert, S. Samukawa, M. Nomura, Impact of nanopillars on phonon dispersion and thermal conductivity of silicon membranes, *Nanoscale* 15 (5) (2023) 2248–2253. doi:10.1039/D2NR06266F.
- [66] H. Wang, Y. Cheng, Z. Fan, Y. Guo, Z. Zhang, M. Bescond, M. Nomura, T. Ala-Nissila, S. Volz, S. Xiong, Anomalous thermal conductivity enhancement in low dimensional resonant nanostructures due to imperfections, *Nanoscale* 13 (22) (2021) 10010–10015. doi:10.1039/D1NR01679B.
- [67] R. Saito, G. Dresselhaus, M. S. Dresselhaus, *Physical Properties of Carbon Nanotubes*, repr Edition, Imperial College Press, London, 1998.
- [68] J. Zimmermann, P. Pavone, G. Cuniberti, Vibrational modes and low-temperature thermal properties of graphene and carbon nanotubes: Minimal force-constant model, *Phys. Rev. B* 78 (4) (2008) 045410. doi:10.1103/PhysRevB.78.045410.
- [69] M. Mohr, J. Maultzsch, E. Dobardžić, S. Reich, I. Milošević, M. Damjanović, A. Bosak, M. Krisch, C. Thomsen, Phonon dispersion of graphite by inelastic x-ray scattering, *Phys. Rev. B* 76 (3) (2007) 035439. doi:10.1103/PhysRevB.76.035439.
- [70] S. Liu, F. Yin, V. I. Khvesyuk, Investigating Anisotropic Three-Phonon Interactions in Graphene's Thermal Conductivity Using Monte Carlo Method, *Int J Thermophys* 46 (2) (2025) 22. doi:10.1007/s10765-024-03498-x.
- [71] S. Mazumder, A. Majumdar, Monte Carlo Study of Phonon Transport in Solid Thin Films Including Dispersion and Polarization, *Journal of Heat Transfer* 123 (4) (2001) 749–759. doi:10.1115/1.1377018.
- [72] D. Lacroix, K. Joulain, D. Lemonnier, Monte Carlo transient phonon transport in silicon and germanium at nanoscales, *Phys. Rev. B* 72 (6) (2005) 064305. doi:10.1103/PhysRevB.72.064305.

- [73] J. Peng, W. R. Deskins, A. El-Azab, Monte-Carlo modeling of phonon thermal transport using DFT-based anisotropic dispersion relations over the full Brillouin zone, Computational Materials Science 211 (2022) 111528. doi:10.1016/j.commatsci.2022.111528.
- [74] A. P. Thompson, H. M. Aktulga, R. Berger, D. S. Bolintineanu, W. M. Brown, P. S. Crozier, P. J. In 'T Veld, A. Kohlmeyer, S. G. Moore, T. D. Nguyen, R. Shan, M. J. Stevens, J. Tranchida, C. Trott, S. J. Plimpton, LAMMPS - a flexible simulation tool for particle-based materials modeling at the atomic, meso, and continuum scales, Computer Physics Communications 271 (2022) 108171. doi:10.1016/j.cpc.2021.108171.
- [75] L. Lindsay, D. A. Broido, Optimized tersoff and brenner empirical potential parameters for lattice dynamics and phonon thermal transport in carbon nanotubes and graphene, Phys. Rev. B 81 (2010) 205441. doi:10.1103/PhysRevB.81.205441.
- [76] J. M. Ziman, Electrons and phonons: the theory of transport phenomena in solids, Oxford university press, 2001.
- [77] S. B. Soffer, Statistical model for the size effect in electrical conduction, Journal of Applied Physics 38 (4) (1967) 1710–1715.
- [78] Y. Hu, T. Feng, X. Gu, Z. Fan, X. Wang, M. Lundstrom, S. S. Shrestha, H. Bao, Unification of nonequilibrium molecular dynamics and the mode-resolved phonon Boltzmann equation for thermal transport simulations, Phys. Rev. B 101 (15) (2020) 155308. doi:10.1103/PhysRevB.101.155308.
- [79] A. Alofi, G. P. Srivastava, Thermal conductivity of graphene and graphite, Phys. Rev. B 87 (11) (2013) 115421. doi:10.1103/PhysRevB.87.115421.
- [80] A. Khan, I. Navid, M. Noshin, H. Uddin, F. Hossain, S. Subrina, Equilibrium Molecular Dynamics (MD) Simulation Study of Thermal Conductivity of Graphene Nanoribbon: A Comparative Study on MD Potentials, Electronics 4 (4) (2015) 1109–1124. doi:10.3390/electronics4041109.

- [81] L. Yang, M. I. Hussein, Vibronics of multi-material nanopillared membranes and impact on the thermal conductivity, *J. Phys.: Condens. Matter* 36 (50) (2024) 505303. doi:10.1088/1361-648X/ad6b6c.